The role of *LMNA* in adipose: a novel mouse model of lipodystrophy based on the Dunnigan-type familial partial lipodystrophy mutation[S]

Kari M. Wojtanik,[1,*] Keith Edgemon,[2,*] Srikant Viswanadha,[3,*] Brigette Lindsey,[4,*] Martin Haluzik,[5,†] Weiping Chen,[3] George Poy,[§] Marc Reitman,[6,] and Constantine Londos[*]**

Laboratory of Cellular and Developmental Biology,* Mouse Metabolic Core,† Genomics Core Laboratory,§ and Diabetes Branch,** National Institute of Diabetes and Digestive and Kidney Diseases, National Institutes of Health, Bethesda, MD 20892

Abstract We investigated the role of *LMNA* in adipose tissue by developing a novel mouse model of lipodystrophy. Transgenic mice were generated that express the *LMNA* mutation that causes familial partial lipodystrophy of the Dunnigan type (FPLD2). The phenotype observed in FPLD-transgenic mice resembles many of the features of human FPLD2, including lack of fat accumulation, insulin resistance, and enlarged, fatty liver. Similar to the human disease, FPLD-transgenic mice appear to develop normally, but after several weeks they are unable to accumulate fat to the same extent as their wild-type littermates. One poorly understood aspect of lipodystrophies is the mechanism of fat loss. To this end, we have examined the effects of the FPLD2 mutation on fat cell function. Contrary to the current literature, which suggests FPLD2 results in a loss of fat, we found that the key mechanism contributing to the lack of fat accumulation involves not a loss, but an apparent inability of the adipose tissue to renew itself. Specifically, preadipocytes are unable to differentiate into mature and fully functional adipocytes. These findings provide insights not only for the treatment of lipodystrophies, but also for the study of adipogenesis, obesity, and insulin resistance.— Wojtanik, K. M., K. Edgemon, S. Viswanadha, B. Lindsey, M. Haluzik, W. Chen, G. Poy, M. Reitman, and C. Londos. **The role of *LMNA* in adipose: a novel mouse model of lipodystrophy based on the Dunnigan-type familial partial lipodystrophy mutation. *J. Lipid Res.* 2009.** 50: **1068–1079.**

Supplementary key words adipocyte differentiation • insulin resistance • lamin A • lamin C • laminopathies • preadipocyte • type 2 diabetes

Type 2 diabetes and insulin resistance are often associated with obesity. However, an extreme paucity of fat, as occurs in lipodystrophies, can also give rise to these syndromes (1). Thus, it has become evident that adipose tissue mass plays a significant role in regulating whole body metabolism (2). Years of research have revealed many new genes and proteins that have been defined as having a key role in regulating adipose tissue metabolism. Despite these revelations, the function of many of these genes in adipose tissue is unclear.

Mutations in the *LMNA* gene have been shown to cause Dunnigan-type familial partial lipodystrophy (FPLD2) (3). Approximately 90% of *LMNA* mutations that cause FPLD2 are localized to exon 8 and occur at amino acid 482 (4). FPLD2 patients present with a variety of clinical symptoms. The hallmark is a progressive loss of subcutaneous fat from the trunk and extremities, and accumulation of subcutaneous fat in the face and neck. The redistribution of adipose tissue is most apparent after puberty (5). The disease is also characterized by a host of metabolic complications, including insulin resistance, type 2 diabetes, dyslipidemia, and hepatic steatosis (6, 7).

LMNA (*Lmna* in mice) encodes for A-type lamins, including the major isoforms lamin A and C (8). They are

This was work was supported by the National Institute of Diabetes and Digestive and Kidney Diseases intramural program, National Institutes of Health.

Manuscript received 19 September 2008 and in revised form 22 January 2009.

Published, JLR Papers in Press, March 19, 2009.
DOI 10.1194/jlr.M800491-JLR200

Abbreviations: FPLD2, FPLD, Familial partial lipodystrophy Dunnigan type; aP2, adipocyte fatty-acid binding protein.

[1] To whom correspondence should be addressed.
e-mail: wojtanikk@niddk.nih.gov
[2] Present address of K. Edgemon: 2921 Deer Hollow Way #114, Fairfax, VA 22031.
e-mail: keith@edgemon.net
[3] Present address of S. Viswanadha: Glenmark Research Center, Plot A-607, T.T.C. Industrial Area, MIDC, Mahape, NAVI MUMBAI 400 709. e-mail: srikantv@glenmarkpharma.com
[4] Present address of B. Lindsey: 78 Bull Street, Charleston, SC 29401.
e-mail: brigette.lindsey@gmail.com
[5] Present address of M. Haluzik: Charles University, Department of Medicine, U nemocnice 1, 12808, Prague, Czech Republic.
e-mail: mhalu@lf1.cuni.cz
[6] Present address of M. Reitman: Merck Research Laboratories, PO Box 2000, RY80M-213, 126 East Lincoln Avenue, Rahway, NJ 07065-0900.
e-mail: marc_reitman@merck.com

[S] The online version of this article (available at http://www.jlr.org) contains supplementary data in the form of two figures.

produced via alternate splicing and share the first 566 amino acids. Mature lamin A is produced from the multi-step post-translational processing of its precursor, prelamin A (9, 10). Lamin A and C, along with other lamin proteins, are primarily localized underneath the inner nuclear membrane and help to form a meshwork called the nuclear lamina (11). Like adipose tissue, the nuclear lamina was once thought to play a silent structural role but has since been demonstrated to have a more active role in regulating gene transcription and expression (12, 13). A-type lamins associate not only with the lamina, but are also distributed throughout the nuclear interior where they have been associated with a range of nuclear bodies, suggesting a role in transcription and RNA processing (14, 15). In addition, they have been reported to associate with a number of transcription factors, including retinoblastoma protein (16) and sterol response element binding protein 1 (SREBP1) (17, 18).

Other mutations in *LMNA*, besides those that cause FPLD2, are responsible for at least 10 other tissue-specific diseases commonly referred to as laminopathies. They include Emery-Dreifuss muscular dystrophy and Hutchison Gilford progeria (4, 19, 20). The participation of lamins in many cell processes and the broad spectrum of diseases that arise from mutations in *LMNA* suggest that lamin proteins have different roles in different somatic cells (14, 21). So, how can genetic variants in a widely expressed nuclear lamin protein result in an adipose tissue-specific phenotype such as FPLD2? The underlying mechanisms are unclear. In an attempt to better understand the role of *LMNA* in adipose tissue, we generated transgenic mice that specifically express, in adipocytes, either human lamin A or C containing the common R482Q FPLD human mutation.

In this paper, we describe the phenotype of our *LMNA*-transgenic mouse, which shares a number of morphological and clinical characteristics with the FPLD2 human patient. Despite the plethora of clinical data for the human patient, the mechanism of lipodystrophy and the role of *LMNA* in adipose and FPLD2 remain unclear. To this end, we have studied the effects of the FPLD2 mutation on fat cell function and found that while there appear to be no defects in lipolysis, there are significant defects in adipocyte differentiation. An understanding of the pathogenesis of a monogenic disorder like FPLD2 and the role of *LMNA* in adipose will provide insights not only into lipodystrophies, but also into the mechanisms of adipose tissue maintenance and insulin resistance as it occurs in obesity.

MATERIALS AND METHODS

Generation of *LMNA* transgenic mice

The plasmids directing fat specific expression of wild-type and mutant lamin A or C were constructed by the use of standard cloning procedures as follows. Human lamin cDNA was obtained from Dr. Robert Goldman (Northwestern University) in *E. coli* expression vector pBR322 (NEB). The lamin A/C sequence was isolated as a BamHI-XbaI fragment. A KpnI site was incorporated between the BamHI and start site, and an XmaI site was incorporated between the stop and XbaI site to facilitate cloning. The modified lamin A fragment was cloned into a pBLuescriptKS+ vector containing the aP2 promoter, SV40 splice site and poly (A) site, denoted as Bluescript aP2 A-ZIP/F SV40 poly(A) (22). The lamin A/C mutation was made, changing amino acid 482 from arginine to glutamine using Stratagene Quick Change Site Directed Mutagenesis Kit (Stratagene).

For microinjection, an 11-kb fragment containing the aP2 promoter, wild-type or mutant lamin A or C, and the SV40 splice, and poly(A) sites was obtained free of vector sequences by NotI digestion and gel purification. Transgenic FVB mice were produced by microinjection into male pronuclei and screened by PCR on tail DNA with transgene-specific primers (5′-ACCCCAAGGACTTTCCTTCAGA-3′, and 5′-CATTGATGAGTTTGGACAAACCAC-3′). Mice used for the experiments were the progeny of F_{10} generation or later from a single founder. Two mutant lamin lines were analyzed. One line expressed mutant lamin A, and a second expressed lamin C with the same R482Q mutation. FPLD2 is an autosomal dominant disorder, and to date, only heterozygous or compound heterozygous mutations have been reported. No homozygous patients have been identified (3, 23). Therefore, to mimic the human disease as closely as possible, all transgenic animals used for the study were hemizygous for the transgene. Male animals at the indicated ages were used for all experiments unless otherwise noted. Mice were maintained on a 12-h light/dark cycle. After weaning, mice were fed either a standard chow diet [9% calories from fat from Ziegler Brothers (Rodent NIH-7 chow)] or a high-fat diet [45% calories from fat (Research Diets, Inc.) no. D12451)] as indicated in figure legends. Animal experiments were approved by the NIDDK Animal Care and Use Committee. Histological analysis was performed by American Histological Laboratories.

Immunoblot analysis

Total cell protein was extracted from approximately 700–900 mg of adipose tissue as follows. Tissue was minced with scissors in 1 ml of cold lysis buffer containing 50 mM TrisHCl, pH 7.4, 100 mM NaCl, 1 mM DTT, 1× complete protease inhibitor tablet (Roche Diagnostics) and then homogenized using a glass homogenizer. A final concentration of 0.5% Triton X-100 was added after homogenation. The sample was centrifuged at 12,000 rpm for 15 min in a micro-centrifuge. The fat-free layer below the triglycerides and above the pellet was discarded, and the remaining pellet resuspended in Laemmli's buffer and sheared with a 25-gauge needle. Samples were heated at 95°C for 5 min, and then separated using NuPAGE 4–10% Bis-Tris gels from Invitrogen. Proteins were then transferred to nylon membrane (Invitrogen). Membranes were blocked in a solution of TBS-Tween containing 5% powdered milk. Lamin A and C proteins were detected with goat polyclonal anti-human antibody (sc-6215), diluted 1:200, from Santa Cruz Biotechnology, Inc. β-actin was detected with mouse monoclonal antibody (Santa Cruz Biotechnology, Inc.). An appropriate horseradish peroxidase-conjugated secondary antibody was used, and bands were visualized by enhanced chemiluminescence (Pierce). Samples from human fibroblasts were a generous gift of Dr. Paola Scaffidi and Dr. Tom Misteli (NIH).

Isolation of peritoneal macrophages

Brewer's complete thioglycollate broth (Difco) was prepared as follows. 15 g of dehydrated thioglycollate medium was suspended in 500 ml water and heated until dissolved, just after boiling. The solution was then autoclaved for 20 min at 121°C and then aged for 1–2 months in a dark room at room temperature. Mice were injected with 2.5 ml of Brewer's thioglycollate broth 5 days prior to harvest. Resident peritoneal macrophages were then obtained by intraperitoneal lavage with Dulbecco's phosphate buffered saline. Cells were counted and then spun at 800 *g* for 10 min. Supernatant was removed, and the pellet lysed in

Laemmli's buffer. Samples were heated for 10 min at 95°C and equal cell numbers were analyzed using NuPAGE 4–10% Bis-Tris gels as described in the previous section.

Body composition

Whole body fat, fluid, and lean tissue were measured weekly using the NMR Analyzer Bruker Minispec for live mice (Bruker Optics, Inc.).

Thermogenesis

Core body temperature was measured using a rectal probe (Thermalet TH-5) inserted 1.0 cm deep at ambient room temperature and during exposure to 4°C, during which time mice were caged individually without bedding. Food and water were provided ad libitum. Experiments were performed by the National Institutes of Health NIDDK Mouse Metabolism Core Laboratory.

Blood glucose and serum insulin

Tail blood was collected from postprandial animals at the indicated time points. Serum insulin was determined by RIA (Linco Research Immunoassay) and blood glucose with a Glucometer Elite (Bayer).

Glucose tolerance tests and hyperinsulinemic-euglycemic clamp studies

Overnight-fasted mice were given i.p. glucose (3 mg/g body weight) and tail blood was collected before (time 0) and at the indicated times after injection. Glucose was measured with a Glucometer Elite (Bayer). Hyperinsulinemic-euglycemic clamp studies were performed by the National Institutes of Health NIDDK Mouse Metabolism Core Laboratory as previously described (24).

Isolation of adipocytes

Adipocytes were isolated from fat pads by collagenase digestion according to the Rodbell method (25) as modified by Honnor et al. (26, 27) in solutions containing 500 nM adenosine. Briefly, the suspensions were incubated for 1 h at 37°C and then filtered through a 250 μm nylon mesh to remove undigested tissue. The extract was incubated for 2–3 min at room temperature to allow partitioning of adipocytes from the collagenase digest, and the infranatant was removed. Remaining adipocytes were washed three times in buffer containing adenosine deaminase and phenylisopropyladenosine (PIA). After addition of the final wash, cells were centrifuged for 30 s at 800 *g*, infranatant was removed, and adipocytes were suspended in a buffer containing 3% BSA.

Lipolysis

Adipocyte suspensions were incubated in solutions containing 1.0 units/ml adenosine deaminase plus 100 nM PIA for basal activity or plus 10 μM isoproterenol for stimulated activity. Samples were incubated for 60 min at 37°C. Infranatant was removed and analyzed for glycerol released into the medium.

Glycerol Assay

Glycerol released into the medium was determined by a radiometric assay (28) adapted to microtiter plates (29). Briefly, [γ^{32}P] ATP and 20 μl glycerokinase (Roche) was added to assay buffer containing 2 mM $MgCl_2$, 100 nM triethanolamine-HCl, 2 mg/ml BSA, and 120 μM ATP. Standards and glycerol samples were incubated with the assay buffer in 96-well plates at 37°C for 30 min. An acidic solution of 2N $HClO_4$ plus 0.2 mM H_3PO_4 was added to each well and incubated at 90°C for 30 min. After cooling, 100 mM ammonium molybdate and 200 mM triethanolamine were added to the wells and the plates centrifuged at 1000 *g* for 20 min. Supernatant was removed and glycerol content was measured by liquid scintillation counting. Glycerol concentrations were determined based on the standard curve.

Normalization of cell number

Data from lipolysis assays were normalized to cell number. Adipocyte suspensions were stained with methylene blue and cell diameter measurements obtained with a Zeiss LSM confocal microscope. The diameters of at least 100 cells were measured for each preparation. The average was used to calculate cell volume. Triglycerides were extracted from adipocyte suspensions using Dole's solution. Cell number was calculated by dividing the mean mass per 1 ml of triglycerides by the mean adipocyte volume.

Differentiation of stromal vascular cell fractions

Adipose tissue was digested as described previously, and floating mature adipocytes were removed by aspiration. Erythrocytes were eliminated from the infranatant by incubating in lysis buffer containing 154 mM NH_4Cl, 10 mM $KHCO_3$ and 0.1 mM EDTA for 10 min. The resulting cell suspensions were centrifuged at 350 *g* for 5 min, and sedimented cells were washed twice with DMEM containing 10% FCS, 100 U/ml penicillin, and 100 μg/ml streptomycin. Washed cells were resuspended in the same media, counted, and plated at a density of 0.75×10^4 cells/cm^2 in DMEM containing 4 μM biotin, 200 μM ascorbate, 100 U/ml penicillin, 100 μg/ml streptomycin, and 5% FCS. Cells were maintained in a humidified incubator (5% CO_2) at 37°C. After 24 h, unattached cells were removed with extensive PBS washing. Cells were grown to confluency and induced to differentiate by adding 100 μM indomethacin, 10 μg/ml insulin, and 0.5 mM IBMX. After 48–72 h, IBMX was removed from the medium. Medium was changed every other day. Images were taken using an Axiovert S100 TV microscope (Zeiss). Differentiation was determined by visual inspection for lipid droplet accumulation and Oil Red O staining.

Oil Red O staining

Oil Red O stock solution was made by dissolving 0.7 g Oil Red O (Sigma #O-0625) in 200 ml isopropanol, stirring overnight, filtered with 0.2 μm filter, and stored at 4°C. Working solutions were made by dissolving six parts Oil Red O stock with four parts water and filtering with 0.2 μm filter. Cells were fixed in 10% formalin for 1 h at room temperature, washed with 60% isopropanol, and allowed to dry completely. Cells were incubated with Oil Red O working solution for 10 min and then washed several times with water.

Real-time PCR

RNA was harvested on days 0, 4, and 7 of differentiation using RNeasy system from Qiagen according to manufacturer's instructions. First-strand cDNA synthesis was performed using First Strand cDNA Synthesis kit from Fermentas. Real-time PCR was performed by the National Institutes of Health NIDDK Genomics Core Laboratory using an ABI Prism 7900HT Sequence Detection System (Applied Biosystems). PCR products were amplified using inventoried primer sets for aP2, PPARγ, and CEBPα purchased from Applied Biosystems, with GAPDH used as an endogenous control. The ΔΔCt of the gene of interest was determined after normalizing to control gene, GAPDH. Relative expression was calculated using the formula $2^{-\Delta\Delta Ct}$.

Statistical analysis

Data for body composition were analyzed as a completely randomized design using the MIXED procedure of SAS (Version 9.0). All data are reported as least square means ± SEM. Post hoc tests were performed for body composition data using Bonferroni's

multiple comparisons after the overall differences were found to be significant. All other statistical analyses were performed using two-tailed unpaired *t*-tests (GraphPad and Microsoft Excel).

RESULTS

Generation of FPLD transgenic mouse

Different mutations in the same gene rarely result in numerous seemingly unrelated diseases. Therefore, how unique mutations in the *LMNA* gene lead to an adipose tissue-specific disease like FPLD2, while other mutations do not, is unclear. Therefore, we sought to clarify the function of *LMNA* in adipose tissue by developing a mutant LMNA transgenic mouse. Transgenic mice expressing either human mutant lamin A or C containing the most common FPLD2 mutation, R482Q, were generated as described in "Material and Methods." In nature the R482Q mutation affects both lamin A and C as both proteins are generated via alternative splicing from the same gene. Although transgenic mice retain their wild-type copy of *Lmna*, FPLD2 is an autosomal dominant disorder, and expression of only one mutant copy is sufficient to cause the disease. Expression of the transgene was driven by the aP2 enhancer/promoter to ensure adipose tissue-specific expression and to minimize the confounding effects of mutant protein in other tissues. Adipose tissue expression of human lamin A/C was confirmed with immunoblotting (**Fig. 1A**). Expression of the transgene was not observed in other tissues such as muscle, liver, and spleen (data not shown); however, slight expression was observed in macrophages (Fig. 1B).

Subsequent analysis showed that the phenotype of the lamin C line was similar to lamin A but less profound (see supplementary Fig. I). This may be a consequence of lower protein expression (Fig. 1). Thus, only the data from the lamin A transgenic line, herein called FPLD, is presented in detail. In addition, all results presented here are from male mice. Female mice exhibited the same phenotype as males; however, the differences between transgenic and control females were less pronounced, and the phenotype was not evident until after 33 weeks (data not shown) compared with 14 weeks in males.

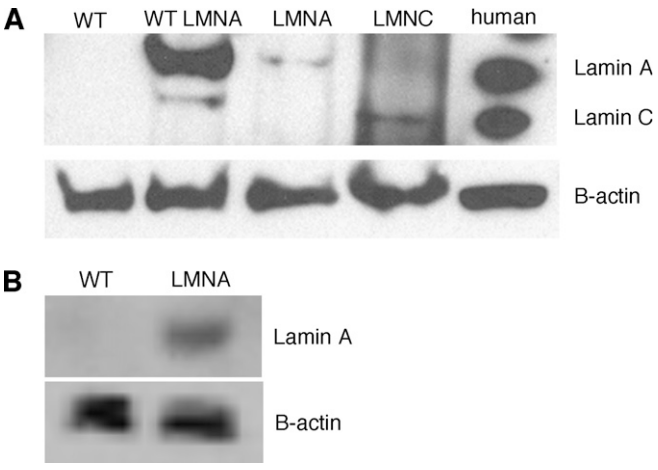

Fig. 1. Expression of lamin A and lamin C in mouse adipose tissue and macrophages. (A) Immunoblot analysis showing expression of lamin A and lamin C protein in adipose tissue isolated from wild-type animals, transgenic animals expressing wild-type human LMNA, transgenic animals expressing mutant human lamin A or lamin C, and human fibroblasts. (B) Immunoblot analysis showing expression of human lamin A in intraperitoneal macrophages isolated from wild-type and transgenic animals expressing mutant human lamin A.

FPLD mice are unable to accumulate fat

Mice were placed on a high-fat diet between 4 and 8 weeks of age and measured weekly for body weight, fat mass, and lean mass. FPLD transgenic mice had no obvious phenotype upon visual inspection and no significant differences in body weight compared with age- and sex-matched wild-type littermates until 41 weeks of age (**Fig. 2A**). At 41 weeks and beyond, control animals became mildly but significantly heavier than FPLD animals. This difference may be due to the fact that FPLD mice have markedly less fat than control mice (Fig. 2B). Body composition analysis by NMR showed that FPLD mice had significantly less fat mass after week 14 (Fig. 2B). While control mice continued to accumulate fat throughout the time-course, FPLD mice appeared to reach a maximum level of fat mass and then plateau. By 63 weeks, FPLD mice on high-fat diet had approximately 60% less fat compared with wild-type animals. Food intake did not differ between the two groups (data not shown). Similar results were seen in mice on a normal chow diet; however, fat mass did not differ significantly between the two groups until after 28 weeks of age (see supplementary Fig. II). These results suggest that certain conditions, such as high-fat feeding, can act to exacerbate the lipodystrophic phenotype.

Gross examination of both white (WAT) and brown adipose tissue (BAT) revealed a marked reduction in epididymal white fat pads (Fig. 2C) and a severe reduction of brown subscapular fat pads (Fig. 2F). Histological examination of epididymal WAT from transgenic mice (Fig. 2E) showed less uniformity in cell size compared with wild-type (Fig. 2D), ranging from hypertrophic to miniscule. In addition, the stroma of epididymal WAT showed significant leukocyte infiltration, indicating an increase in inflammatory processes in transgenic mice. BAT from transgenic animals exhibited significantly enlarged lipid droplets with unilocular versus multilocular deposition (Fig. 2H). This is in contrast to wild-type animals, which showed a strongly uniform distribution of multilocular lipid droplets (Fig. 2G). It is not clear whether the change in BAT architecture is due to defects in the development of BAT or perhaps, in an effort to increase their fat storage capabilities, FPLD mice transdifferentiate BAT to a more WAT-like phenotype. This is suggested by Fig. 2H, where BAT from FPLD animals displays a white-like appearance. This phenomenon has been observed in genetically manipulated animal models (30, 31) and in humans with a reduced potential of adipose precursor cells (32).

Next, the weights of individual fat depots, including epididymal, inguinal, perirenal, retroperitoneal, and brown fat pads were measured. Compared with wild-type, FPLD mice

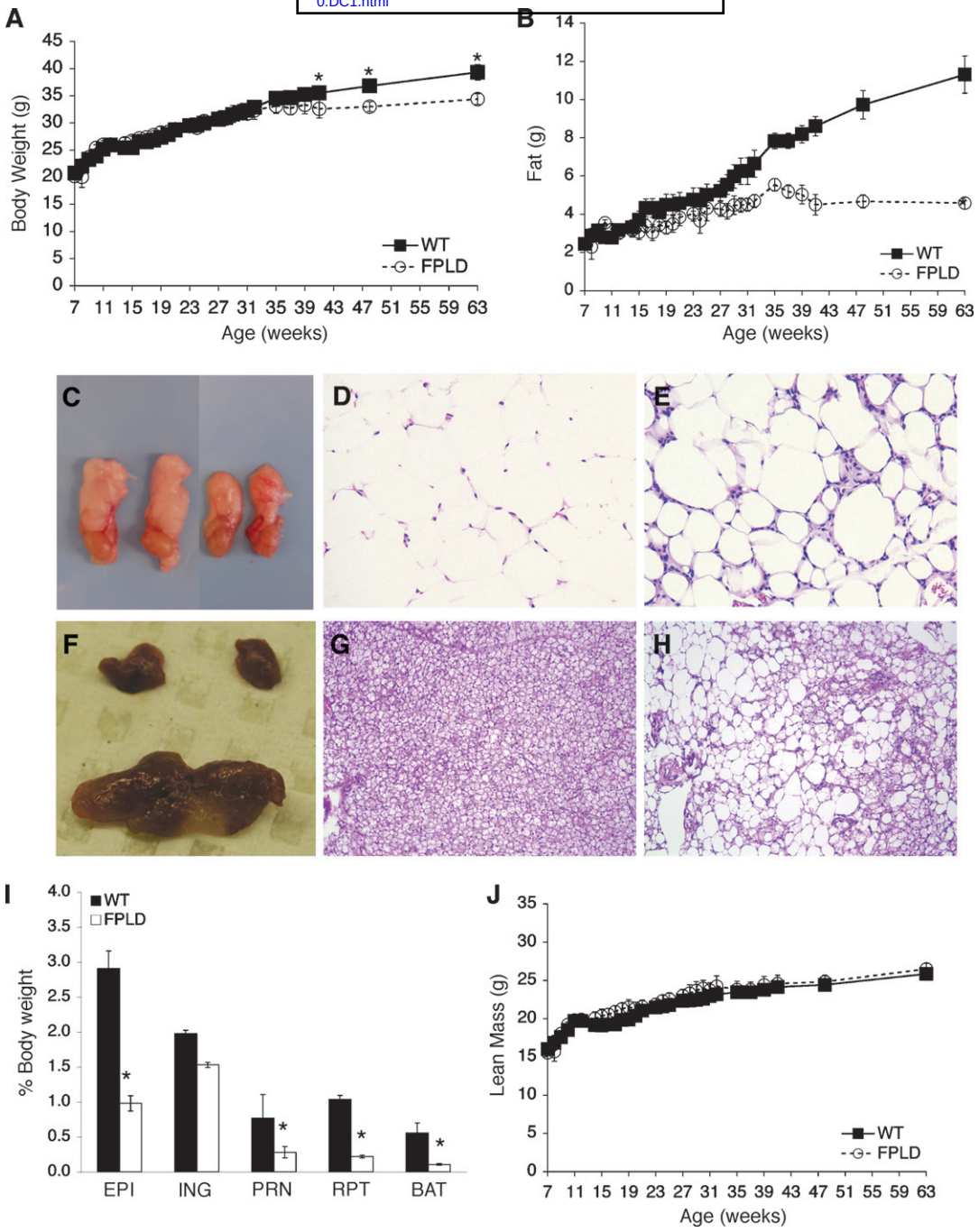

Fig. 2. Body weight, body composition, and adipose histology of FPLD transgenic mice and wild-type littermates on high-fat diet. (A) Body weights of control and FPLD mice. FPLD mice showed no significant differences in body weight until week 41 (week 41, $*P = 0.02$; week 48, $*P = 0.002$; week 63, $*P < 0.0001$). There was no significant difference between the two groups, as a whole, over time. (B) Total body fat of control and FPLD mice. FPLD mice begin to lose their ability to accumulate fat after 14 weeks of age. All data points were significant after 17 weeks and there was a significant difference between the two groups over time ($*P < 0.0001$). After 63 weeks, FPLD mice have approximately 59% less body fat than control littermates. (C) Gross anatomy of epididymal WAT from age and weight matched wild-type (left) and FPLD (right) mice. Hemotoxylin and eosin stained sections of epididymal WAT from wild-type (D) and FPLD (E) mice. (F) Gross anatomy of BAT from wild-type (bottom) and FPLD (top) mice. Hemotoxylin and eosin stained sections of BAT from wild-type (G) and FPLD (H) mice. (I) Weight of individual fat depots expressed as percentage of body weights. FPLD mice had significantly less fat in all depots examined compared with control littermates on both chow and high fat diet ($*P = 0.02 - 0.0001$), except inguinal fat ($P = 0.18$). EPI, epididymal; ING, inguinal; PRN, perirenal; RPT, retro-peritoneal. (J) Total body lean mass of control and FPLD mice. All data are expressed as averages ± SEM (n = 6/group).

had significantly less fat in all depots examined except inguinal (Fig. 2I). Inguinal fat pads from FPLD mice weighed less than those from wild-type mice but did not reach statistical significance.

Since skeletal muscle hypertrophy has been observed in human FPLD2 patients (33), we measured lean mass in FPLD and wild-type mice. Lean mass was mildly, but consistently, higher in FPLD mice compared with wild-type

animals (Fig. 2J), although the values did not reach statistical significance unless expressed as percent of body weight. It is not apparent why skeletal muscle hypertrophy is not as robust in the transgenic animal as it is in the human disease. One speculation is that adipose-specific expression of the FPLD2 mutation, as occurs in the transgenic mice, may lessen the effects of the mutation in other tissues, such as muscle, where it is not expressed.

One concern was that expression of the transgene, irrespective of the mutation, was sufficient to cause the observed phenotype. This was based on recent cell culture studies from Boguslavsky et al. (34), which suggest that overexpression of wild-type lamin A may lead to a FPLD2 phenotype. To address this, we generated a transgenic mouse in which aP2 drives expression of wild-type human lamin A. Thus, transgenic mice expressed both wild-type mouse and human lamin A. Bruker and weight analysis showed that body composition of wild-type lamin-transgenic mice did not differ from wild-type littermates (**Fig. 3**), confirming that expression of the mutant lamin A, and not over-expression of wild-type lamin A, causes the phenotype. In addition, we performed a gross examination of the livers from wild-type lamin-transgenic animals and found no evidence of steatosis (data not shown), which is commonly observed in FPLD2.

FPLD mice have decreased insulin sensitivity and fatty liver

Patients affected with FPLD2 present with metabolic complications such as glucose intolerance, insulin resistance, and fatty liver (35–37). These parameters were examined in our FPLD transgenic mouse. Compared with wild-type littermates, FPLD mice showed moderately increased blood glucose levels and significantly increased serum insulin levels by week 18 (**Fig. 4A**). Glucose tolerance tests performed at week 22 showed glucose levels to be higher in FPLD mice than in controls at all time points (Fig. 4B). The above results are consistent with insulin resistance in FPLD mice. These results were confirmed in hyperinsulinemic-euglycemic clamp studies performed on 32-week-old mice. Prior to the clamp, FPLD mice had similar endogenous glucose production rates. Glucose infusion rates and rates of whole-body glucose uptake and glycogen synthesis were significantly lower in FPLD mice (Fig. 4C), with 25% less glucose uptake in muscle and more than 30% less glucose uptake in WAT (Fig. 4D). Overall, these findings demonstrate that whole-body insulin resistance is occurring and that FPLD mice have altered insulin sensitivity in multiple tissues (liver, muscle, and WAT).

Since hepatic steatosis is part of the clinical phenotype of FPLD2, we examined the liver weight, pathology, and fat content in FPLD mice and control littermates. Upon gross examination, livers from FPLD mice showed the characteristic pallor of steatosis (**Fig. 5A**). They were visibly enlarged, yellow, and had a blotchy appearance. Histological analysis (Fig. 5B) revealed massive infiltration of large lipid vacuoles within hepatocytes of FPLD mice (right panel) when compared with wild-type (left panel). Liver weights were 35% higher (Fig. 5C) in FPLD mice and had 35% more lipid than control mice (Fig. 5D). The mechanism for fatty liver is likely indirect and a consequence of the inability of adipose tissue to adequately store fat.

FPLD mice display defects in thermogenesis

Non-shivering thermogenesis in BAT is the primary mechanism of heat production in small mammals, such as mice and newborn humans. Although BAT is widely distributed throughout the body, the largest depot in the mouse is found in the interscapular region (38). FPLD animals have very little to no interscapular BAT. In addition, BAT from these animals displays abnormal lipid droplet organization (Fig. 2H), indicative of reduced thermogenic capacity. To determine if FPLD animals have decreased thermogenic capabilities, FPLD and wild-type mice were housed at 4°C and rectal temperatures were measured over 7 h. After 4 h at 4°C, FPLD mice and their wild-type littermates were unable to maintain their core temperature (**Fig. 6**), suggesting reduced thermogenic capacity. While the importance of BAT during the perinatal period in humans has been well documented, its metabolic significance in adults has only recently become evident (39). In addition there has been no link, as yet, to defects in BAT cells or heat production in FPLD2 patients. However, there have been reports of increased energy expenditure in FPLD2 patients (40),

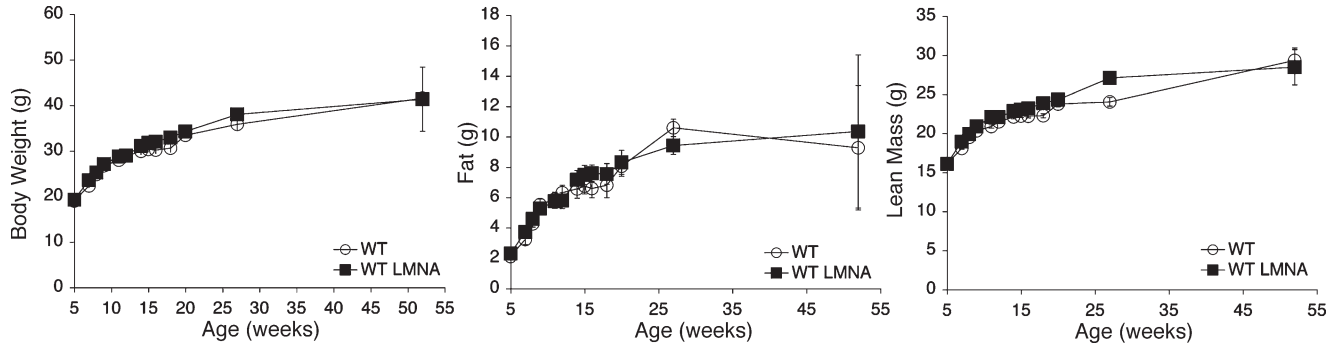

Fig. 3. Body weight and composition of transgenic mice on a high-fat diet, expressing wild-type human lamin A protein. Transgenic mice expressing the wild-type human lamin A display no significant differences in body weight, fat mass, or muscle mass compared with wild-type control littermates, which express no human isoform.

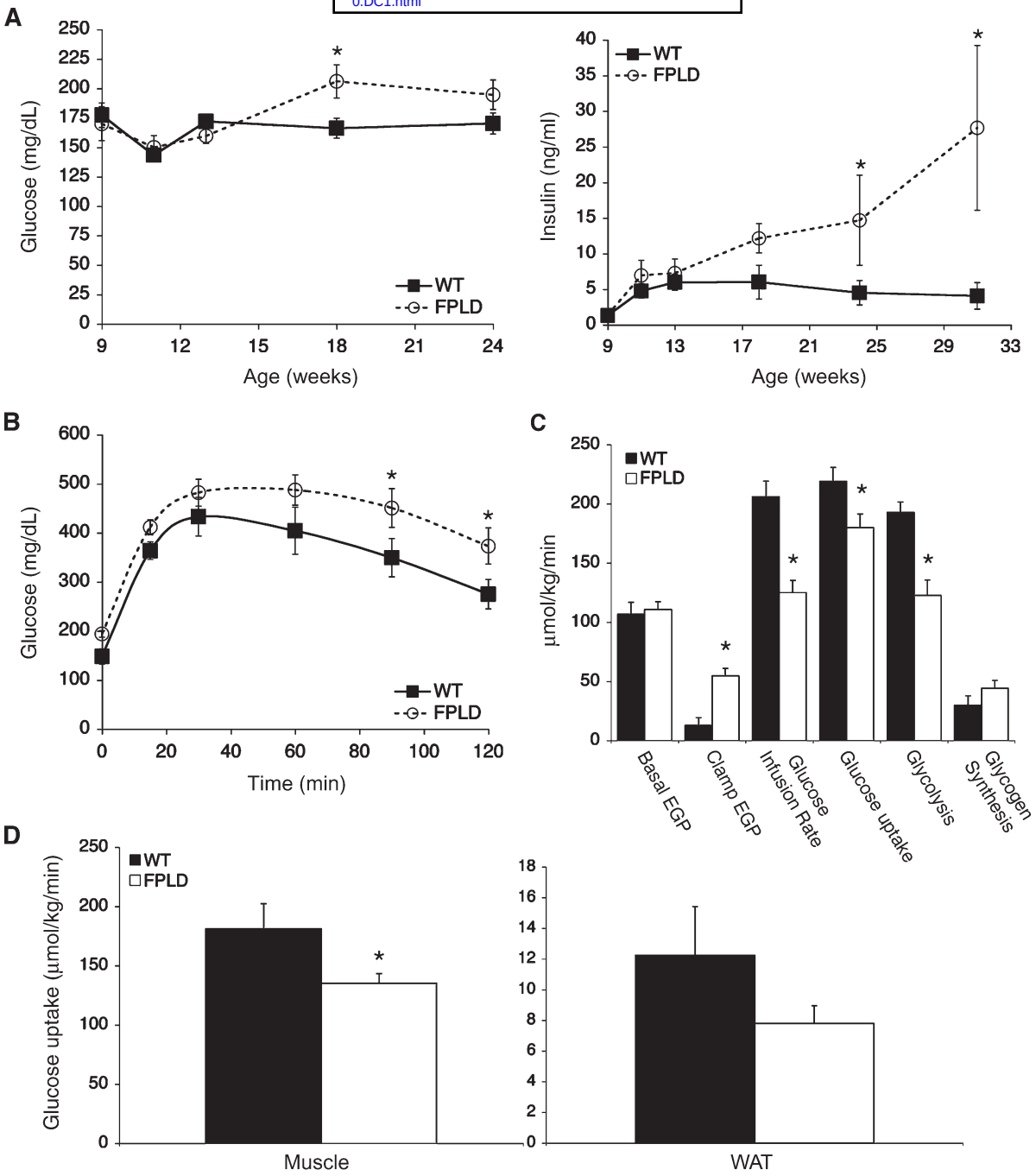

Fig. 4. Glucose tolerance and insulin sensitivity. (A) Blood glucose (left) and serum insulin (right) were measured at the indicated time points from postprandial control and FPLD mice on high-fat diet (n = 5–7/group). FPLD mice do not show dramatic changes in blood glucose levels compared with controls, but have significantly higher serum insulin levels at 24 and 31 weeks (*$P = 0.04$ and *$P < 0.0001$, respectively). (B) Glucose tolerance test using 3 mg/g glucose in overnight-fasted control and FPLD mice on high-fat diet (n = 5–7/group). FPLD mice show significantly higher blood glucose levels at 90 and 120 min during a glucose tolerance test (*$P = 0.03$ and 0.04, respectively). (C) Whole-body glucose fluxes in 32 week old control and FPLD mice during euglycemic-hyperinsulinemic clamp studies (n = 4–5/group). Clamp EGP, $P = 0.002$; glucose uptake, $P = 0.05$; glycolysis, $P = 0.004$. EGP, endogenous glucose production. (D) Tissue glucose uptake rates during clamp studies. FPLD mice have a 25–30% decease in insulin sensitivity in muscle (*$P = 0.03$) and WAT. All data are expressed as averages ± SEM.

suggesting a link between nonfunctional BAT in FPLD mice and the human disease.

Adipocytes from FPLD mice have a normal lipolytic response

One poorly understood aspect of FPLD2 is the mechanism of fat loss. Adipose tissue may lose its capacity to store fat due to a number of factors including increased lipolysis. Lipolysis studies with isolated adipocytes demonstrated that FPLD mice do not stop accumulating fat due to an increase in lipolytic activity. When normalized for cell number and size, basal glycerol release was similar in FPLD and wild-type mice (**Fig. 7**). In addition, both groups showed a similar increase in lipolysis upon stimulation with a β-adrenergic

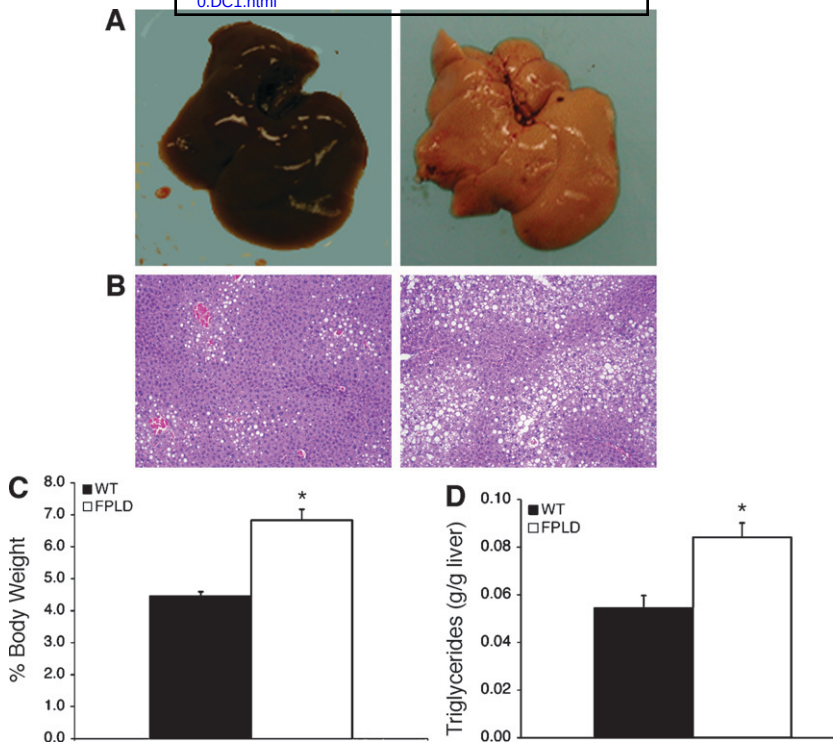

Fig. 5. Liver histology, weight, and triglyceride content. (A) Gross pathology of livers from representative control (left) and FPLD (right) mice at 32 weeks of age on a high fat diet. (B) Hemotoxylin and eosin stained sections of livers from representative control (left) and FPLD (right) mice at 32 weeks of age on high-fat diet. (C) Liver weight expressed as percentage of total body weight from control and FPLD mice at 32 weeks of age on a high-fat diet (n = 6/group). FPLD livers weighed significantly more than livers from control animals (*$P = 0.0004$). (D) Triglyceride content of livers from control and FPLD mice at 32 weeks of age on high-fat diet (n = 4–6/group). Livers from FPLD mice had significantly more triglyceride per gram of liver than control mice (*$P = 0.006$). Data are expressed as averages ± SEM.

agonist. This suggests that overactive hydrolysis of triglycerides in FPLD mice does not likely contribute to their inability to accumulate fat.

FPLD mice display defects in adipocyte differentiation

A second mechanism by which adipose tissue may lose its capacity to store triglycerides is a defect in the ability of precursor cells to differentiate into mature adipocytes and accumulate lipid. To address the hypothesis that FPLD mice have defects in adipocyte differentiation, stromal vascular fractions isolated from epididymal fat pads at 40 weeks were plated onto tissue culture dishes and subsequently induced to differentiate. No differences in the time to reach confluence (corresponds to day 0 of adipocyte differentiation)

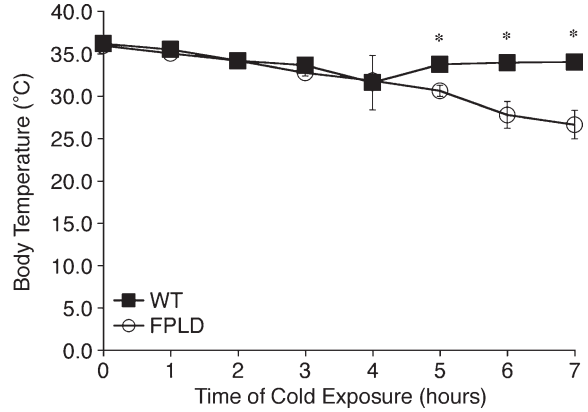

Fig. 6. Thermogenesis in wild-type and FPLD mice at 32 weeks of age. Changes in core body temperature were measured during exposure to 4°C for 7 h. FPLD mice have significantly lower body temperatures at 5, 6, and 7 h compared with wild-type littermates (*$P = 0.01$, 0.01, and 0.008, respectively). Data are expressed as averages ± SEM, n = 4–6 per group.

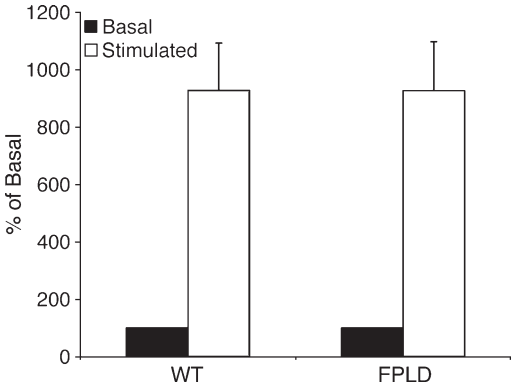

Fig. 7. Lipolysis of triglycerides in adipocytes isolated from epididymal fat pads from control and FPLD mice at 32 weeks of age on a high-fat diet. Lipolysis was measured under basal (unstimulated) and stimulated (isoproterenol) conditions and expressed as percent of basal activity (nmol of glycerol release per 10^6 cells). Data are expressed as averages ± SEM, n = 6/group. There is no significant difference between control and transgenic animals.

were observed between preparations from either FPLD or wild-type mice (**Fig. 8A**, panels A, B, F, and G). Cells from both animals exhibited the same fibroblastic morphology, and no apparent lipid droplets were observed at confluence. However, cells from wild-type animals exhibited morphological changes between day 3 and day 7 of differentiation. They developed a rounded shape consistent with maturing adipocytes and accumulated numerous lipid droplets in their cytoplasm (Fig. 8A, panels C and D). In contrast, cells from FPLD animals contained considerably fewer lipid droplets, and many cells retained their fibroblastic shape (panels H and I). These data were confirmed by Oil Red O staining shown in panels E and J. These results suggest that lipid accumulation was significantly delayed and/or limited in preadipocytes from FPLD mice. They also indicate that defects in adipocyte differentiation exist in these cells.

To reinforce this hypothesis, we examined the expression of several markers of adipocyte differentiation using real-time PCR (Fig. 8B). We found that expression of ap2, a fatty acid binding protein that is a known marker of adipocyte differentiation (41), increased from day 0 to day 7 in wild-type cells. In contrast, expression levels of ap2 did not dramatically increase in FPLD cells. The differences between the two groups were significant by day 4 of differentiation. Expression of PPARγ and CEBPα, which is also known to increase with adipocyte differentiation (42), showed reduced levels of expression in FPLD cells compared with wild-type cells. While these differences appear

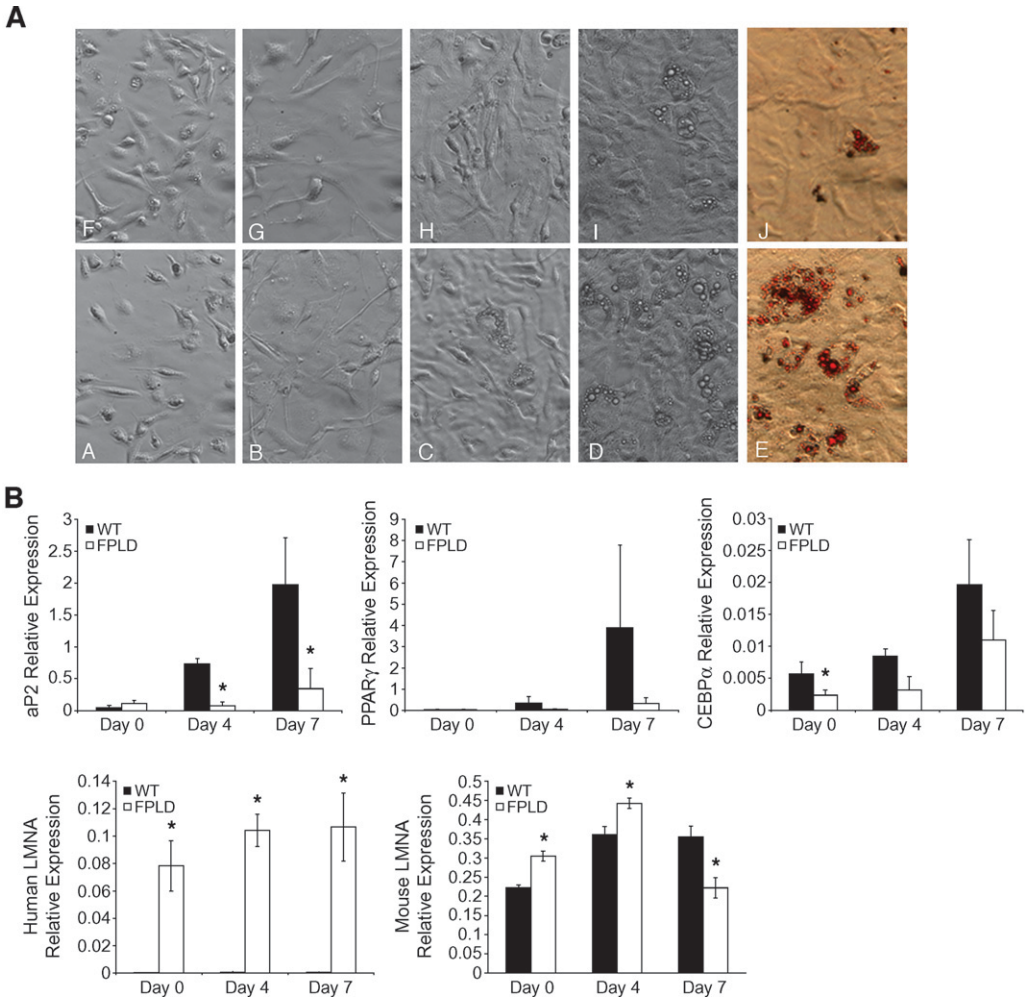

Fig. 8. Adipocyte differentiation and gene expression in cells isolated from control (A–E) or FPLD (F–J) mice at 30 weeks of age on a high-fat diet. (A) Stromal vascular fractions isolated from epididymal fat fads were cultured and induced to differentiate over a period of 7-8 days. Panels A and F, one day after culture; B and G, day 0 of differentiation; C and H, day 4 of differentiation; D and I, day 7 of differentiation; E and J, Oil red O staining at day 7 of differentiation. By day 7 of differentiation, cells isolated from FPLD mice show clear defects in their ability to differentiate into mature adipocytes and accumulate lipid. Figures shown are representative of 4 independent experiments, where n = 3/group/experiment. (B) Real-time PCR of adipocyte differentiation marker genes. Real-time PCR quantitation was performed using RNA harvested on day 0, 4, and 7 of differentiation. Amplification of each sample was performed in triplicate or quadruplicate and normalized to GAPDH. aP2, $*P = 0.002$ and 0.004, respectively; CEBPα, $*P = 0.04$; human LMNA, $*P = 0.0009$, 0.001, and 0.0003, respectively; mouse LMNA, $*P = 0.001$, 0.02, 2.65×10^{-6}, respectively. Data are expressed as relative expression compared with control gene, GAPDH, ± SEM, n = 3–6/group.

dramatic, not all of the data were statistically significant, likely due to biological variability. Nonetheless, these results indicate that preadipocytes from FPLD mice are unable to develop into mature adipocytes and accumulate lipid. This suggests that the major defect that makes FPLD mice unable to accumulate fat is an inability to maintain a mature pool of adipocytes.

One concern was that low levels of aP2 expression in cells from FPLD animals could result in low levels of expression of the mutant LMNA transgene during the differentiation process. To address this and confirm that our transgene was being expressed in differentiating stromal vascular cells, we measured expression of the mutant human LMNA transgene, as well as expression of endogenous mouse LMNA (Fig. 8B). Endogenous mouse LMNA was expressed at slightly higher levels compared with expression of human LMNA. As expected, there was no expression of human LMNA in wild-type mice. In contrast, FPLD mice showed robust expression of the human transgene throughout differentiation. The two groups were significantly different from each other at each time point ($P = 0.0009$, 0.001, and 0.0003, respectively). These data confirm that expression of transgenic ap2 is adequate to drive expression of the mutant LMNA transgene despite reduced expression of endogenous ap2. Expression of endogenous mouse LMNA increases with differentiation in cells from both groups with a very slight decrease in wild-type cells and a moderate decrease in FPLD cells at day 7 of differentiation. Our results are consistent with previous studies demonstrating that, in most fat depots, LMNA expression generally increases with cell differentiation, whereas other fat depots show an initial increase in LMNA expression followed by a decrease at later time points (43). While the differences in expression of endogenous mouse LMNA are not dramatic between the two groups, the data are significant. The reasons for these differences are not clear, but perhaps FPLD mice try to compensate for the presence of mutant LMNA by increasing expression of wild-type mouse LMNA.

DISCUSSION

The results reported here implicate impaired adipocyte differentiation as the basis for lipodystrophy in FPLD2. This is in contrast to the current literature that suggests adipose tissue is lost during the course of the disease. We have developed a transgenic mouse that expresses an adipose tissue-specific mutant form of lamin A, which causes FPLD2 in humans. The syndrome observed in the FPLD transgenic mouse resembles many of the features of human FPLD2. Common aspects include lack of fat accumulation, insulin resistance, muscular hypertrophy, and an enlarged, fatty liver. The redistribution of fat in mice does not appear to be as defined as in humans. Human FPLD2 patients lose fat primarily from the trunk and extremities, whereas mice appear to have defects in almost all fat depots. Currently there is no finite evidence to explain differences in fat distribution in humans, although many studies have implicated fat depot-specific differences in PPARγ expression (44, 45). Perhaps, the fat redistribution that occurs in FPLD mice, compared with human FPLD2, differs because PPARγ expression varies in their respective fat depots. In addition, just as gene expression profiles differ among fat depots, so does adipocyte differentiation (46). Therefore, the depots that are most sensitive to changes in the adipogenic gene profile and differentiation will be the depots most likely affected by the LMNA mutation, and these may differ in mice versus humans.

Adipose tissue in FPLD2 patients develops normally. The lipodystrophy typically manifests at the time of puberty with a gradual loss of adipose tissue (5). FPLD mice appear to develop in the same manner; however, the phenotype does not manifest at sexual maturity but at a much later time. This suggests that puberty may not be requisite for the phenotype to develop in mice. The difference in phenotype onset may also be due to the tissue-specific, rather than global, expression of the mutant gene. The most prominent difference between humans with FPLD2 and our FPLD mice relates to gender. Metabolic complications such as diabetes, hyperlipidemia, and cardiovascular disease occur more often in women than in men (35, 47). We found the FPLD2 phenotype to be more prominent in male mice than in female mice. One explanation may be that FVB female mice are more resistant to diet-induced obesity than male mice (48, 49) and thus more resilient to excess fat challenges.

Another interesting observation was the time lag at which the phenotype emerges on the chow diet compared with the high-fat diet with respect to both body composition and decreased insulin sensitivity. This suggests that the FPLD2 phenotype may arise when the energy storage demands change (as in puberty) or outweigh the energy storage capacity (as with high-fat diet). These increased demands or changes in fat distribution exacerbate or accelerate the appearance of the phenotype. One key question in human FPLD2 is whether the changes in fat distribution precede the metabolic defects or whether maldistribution of fat is secondary to some other metabolic defect caused by the LMNA mutation. While our mouse model cannot completely rule out that failure to regenerate adipose tissue may be partially caused or exacerbated by defects in metabolic pathways, our current data suggest the maldistribution of fat precedes the metabolic disturbances. Fat mass in FPLD mice begins to deviate from wild-type littermates around 14 weeks of age. The metabolic disturbances appear after this time, at around 20 weeks of age, and do not appear significant until after 24 weeks of age. It should also be noted that in other mouse models of lipodystrophy, such as the aP2 SREBP-1c transgenic and AZIP mouse (22, 50, 51), as well as human studies of FPLD2 patients (52), leptin or troglitazone administration was able to restore insulin sensitivity and other metabolic parameters but not adipose mass. This suggests that a lack of adipose tissue is at least initially responsible for the metabolic defects and not vice versa. The issue of whether maldistribution of fat is a direct or secondary effect could potentially be resolved with this model once a better understanding of the role of lamins in adipogensis is clear.

Two major mechanisms may contribute to the inability of FPLD mice to accumulate fat: abnormal increases in the breakdown of adipose fat stores or an inability of adipocyte precursors to differentiate into mature adipocytes and accumulate lipid. We found that increased lipolysis did not contribute to fat loss in FPLD mice. However, preadipocytes from FPLD mice showed clear defects in differentiation. Microscopic analysis revealed that most preadipocytes isolated from FPLD mice retained their fibroblastic appearance and failed to accumulate significant lipid even after 7 days of differentiation. These results were confirmed with real-time PCR, which showed reduced expression of prodifferentiation factors, such as aP2, PPARγ, and CEBPα.

When challenged with excess energy load, adipose tissue must recruit a new pool of adipocytes when existing adipocytes reach their maximum capacity for storing lipid. Because FPLD animals cannot recruit a mature pool of adipocytes, they eventually lose their capacity to accumulate fat. The mechanisms underlying these differentiation defects are not clear. Nonetheless, it is clear that challenging with high-fat diet can exacerbate the defects in these mice. This is evidenced by the differences we saw in response to chow versus high-fat diet. One hypothesis is that recruitment of new preadipocytes, in spite of the fact that they are unable to fully mature and store much lipid, is sufficient to accommodate excess energy stores for some time. A threshold is reached, at which time adipocytes cannot keep up with the excess energy demands and cannot accumulate more fat. A second hypothesis is that the pool of preadipocytes is finite. In a normal animal, a new pool of adipocytes is recruited in response to excess fat load. Conversely, preadipocytes from FPLD animals are not able to fully mature, causing a more rapid recruitment and turnover of precursor cells. If this pool is finite, then eventually adipocyte precursors will run out, thus preventing fat accumulation in adipose tissue. This hypothesis is supported by the recent development of an inducible fatless mouse model called FAT-ATTAC mouse (53). These studies showed that functional adipocytes could be recovered after cessation of treatment that causes their ablation. However, recent data has shown that if treatment lasted more than 12–14 weeks, the effects were not fully reversible, suggesting preadipocyte pools can be depleted (P. Scherer, 2007, personal communication).

It is important that we do not exclude factors, other than differentiation defects, which may contribute the FPLD2 phenotype. aP2 is coexpressed in adipocytes and macrophages. Since the mutant LMNA transgene is driven by an ap2 promoter, it was not unexpected that it was expressed in both adipose tissue and macrophages. Macrophage expression, however, was very slight. This is due to the fact that adipocytes express approximately 10,000-fold higher levels of aP2 compared with macrophages (54). One possibility is that macrophage infiltration and subsequent adipose cell death contribute to the lack of fat accumulation. While this mechanism may not be a major contributor to the phenotype under chow diet conditions (see supplementary Fig. II), it may help to exacerbate the phenotype under high-fat diet conditions, where macrophage infiltration could be likely (55, 56).

So, how do mutations in lamin A lead to defective adipocyte differentiation? One clue comes from studies by Capanni et al. (17). They have shown that prelamin A, the immature form of lamin A, is processed at a reduced rate and accumulates in FPLD2 fibroblasts. In addition, they demonstrate that SREBP1, a transcription factor that mediates adipocyte differentiation, interacts with prelamin A. Overexpression of prelamin A sequesters SREBP1 at the adipocyte nuclear envelope, thus preventing its translocation to the nuclear interior. These events were concomitant with impaired adipocyte differentiation. Perhaps FPLD transgenic mice have accumulation of prelamin A, which binds SREBP1 and prevents it from entering the nucleus. This would subsequently preclude activation of other transcription factors that mediate adipocyte differentiation, such as PPARγ and CEBPα. While no accumulation of prelamin A was observed in our initial immunoblot analysis, studies are ongoing to determine if this is a plausible mechanism in our FPLD mouse.

The authors would like to thank Oksana Gavrilova for technical assistance with Bruker measurements, thermogenesis measurements, and helpful discussions concerning experimental design; Alan Kimmel and Sam Cushman for reading the manuscript and helpful discussions; Paola Scaffidi for providing human fibroblasts for immunoblotting; Matthew McAviney for his assistance with mouse genotyping; and Lyn Gauthier for assistance in generating the wild-type transgenic mouse.

REFERENCES

1. Agarwal, A. K., and A. Garg. 2006. Genetic basis of lipodystrophies and management of metabolic complications. *Annu. Rev. Med.* **57:** 297–311.
2. Rajala, M. W., and P. E. Scherer. 2003. Minireview: The adipocyte–at the crossroads of energy homeostasis, inflammation, and atherosclerosis. *Endocrinology.* **144:** 3765–3773.
3. Cao, H., and R. A. Hegele. 2000. Nuclear lamin A/C R482Q mutation in canadian kindreds with Dunnigan-type familial partial lipodystrophy. *Hum. Mol. Genet.* **9:** 109–112.
4. Jacob, K. N., and A. Garg. 2006. Laminopathies: multisystem dystrophy syndromes. *Mol. Genet. Metab.* **87:** 289–302.
5. Garg, A., R. M. Peshock, and J. L. Fleckenstein. 1999. Adipose tissue distribution pattern in patients with familial partial lipodystrophy (Dunnigan variety). *J. Clin. Endocrinol. Metab.* **84:** 170–174.
6. Hegele, R. A., H. Cao, C. M. Anderson, and I. M. Hramiak. 2000. Heterogeneity of nuclear lamin A mutations in Dunnigan-type familial partial lipodystrophy. *J. Clin. Endocrinol. Metab.* **85:** 3431–3435.
7. Haque, W. A., F. Vuitch, and A. Garg. 2002. Post-mortem findings in familial partial lipodystrophy, Dunnigan variety. *Diabet. Med.* **19:** 1022–1025.
8. Lin, F., and H. J. Worman. 1993. Structural organization of the human gene encoding nuclear lamin A and nuclear lamin C. *J. Biol. Chem.* **268:** 16321–16326.
9. Corrigan, D. P., D. Kuszczak, A. E. Rusinol, D. P. Thewke, C. A. Hrycyna, S. Michaelis, and M. S. Sinensky. 2005. Prelamin A endoproteolytic processing in vitro by recombinant Zmpste24. *Biochem. J.* **387:** 129–138.
10. Sasseville, A. M., and Y. Raymond. 1995. Lamin A precursor is localized to intranuclear foci. *J. Cell Sci.* **108:** 273–285.
11. Aebi, U., J. Cohn, L. Buhle, and L. Gerace. 1986. The nuclear lamina is a meshwork of intermediate-type filaments. *Nature.* **323:** 560–564.
12. Hutchison, C. J., and H. J. Worman. 2004. A-type lamins: guardians of the soma? *Nat. Cell Biol.* **6:** 1062–1067.

13. Moir, R. D., T. P. Spann, and R. D. Goldman. 1995. The dynamic properties and possible functions of nuclear lamins. *Int. Rev. Cytol.* **162B:** 141–182.
14. Hutchison, C. J. 2002. Lamins: building blocks or regulators of gene expression? *Nat. Rev. Mol. Cell Biol.* **3:** 848–858.
15. Kennedy, B. K., D. A. Barbie, M. Classon, N. Dyson, and E. Harlow. 2000. Nuclear organization of DNA replication in primary mammalian cells. *Genes Dev.* **14:** 2855–2868.
16. Ozaki, T., M. Saijo, K. Murakami, H. Enomoto, Y. Taya, and S. Sakiyama. 1994. Complex formation between lamin A and the retinoblastoma gene product: identification of the domain on lamin A required for its interaction. *Oncogene.* **9:** 2649–2653.
17. Capanni, C., E. Mattioli, M. Columbaro, E. Lucarelli, V. K. Parnaik, G. Novelli, M. Wehnert, V. Cenni, N. M. Maraldi, S. Squarzoni, et al. 2005. Altered pre-lamin A processing is a common mechanism leading to lipodystrophy. *Hum. Mol. Genet.* **14:** 1489–1502.
18. Lloyd, D. J., R. C. Trembath, and S. Shackleton. 2002. A novel interaction between lamin A and SREBP1: implications for partial lipodystrophy and other laminopathies. *Hum. Mol. Genet.* **11:** 769–777.
19. Genschel, J., and H. H. Schmidt. 2000. Mutations in the LMNA gene encoding lamin A/C. *Hum. Mutat.* **16:** 451–459.
20. Mounkes, L., S. Kozlov, B. Burke, and C. L. Stewart. 2003. The laminopathies: nuclear structure meets disease. *Curr. Opin. Genet. Dev.* **13:** 223–230.
21. Mattout, A., T. Dechat, S. A. Adam, R. D. Goldman, and Y. Gruenbaum. 2006. Nuclear lamins, diseases and aging. *Curr. Opin. Cell Biol.* **18:** 335–341.
22. Moitra, J., M. M. Mason, M. Olive, D. Krylov, O. Gavrilova, B. Marcus-Samuels, L. Feigenbaum, E. Lee, T. Aoyama, M. Eckhaus, et al. 1998. Life without white fat: a transgenic mouse. *Genes Dev.* **12:** 3168–3181.
23. Speckman, R. A., A. Garg, F. Du, L. Bennett, R. Veile, E. Arioglu, S. I. Taylor, M. Lovett, and A. M. Bowcock. 2000. Mutational and haplotype analyses of families with familial partial lipodystrophy (Dunnigan variety) reveal recurrent missense mutations in the globular C-terminal domain of lamin A/C. *Am. J. Hum. Genet.* **66:** 1192–1198.
24. Chen, M., M. Haluzik, N. J. Wolf, J. Lorenzo, K. R. Dietz, M. L. Reitman, and L. S. Weinstein. 2004. Increased insulin sensitivity in paternal Gnas knockout mice is associated with increased lipid clearance. *Endocrinology.* **145:** 4094–4102.
25. Rodbell, M. 1964. Metabolism of isolated fat cells. I. Effects of hormones on glucose metabolism and lipolysis. *J. Biol. Chem.* **239:** 375–380.
26. Honnor, R. C., G. S. Dhillon, and C. Londos. 1985. cAMP-dependent protein kinase and lipolysis in rat adipocytes. II. Definition of steady-state relationship with lipolytic and antilipolytic modulators. *J. Biol. Chem.* **260:** 15130–15138.
27. Honnor, R. C., G. S. Dhillon, and C. Londos. 1985. cAMP-dependent protein kinase and lipolysis in rat adipocytes. I. Cell preparation, manipulation, and predictability in behavior. *J. Biol. Chem.* **260:** 15122–15129.
28. Bradley, D. C., and H. R. Kaslow. 1989. Radiometric assays for glycerol, glucose, and glycogen. *Anal. Biochem.* **180:** 11–16.
29. Brasaemle, D. L., D. M. Levin, D. C. Adler-Wailes, and C. Londos. 2000. The lipolytic stimulation of 3T3–L1 adipocytes promotes the translocation of hormone-sensitive lipase to the surfaces of lipid storage droplets. *Biochim. Biophys. Acta.* **1483:** 251–262.
30. Kang, S., L. Bajnok, K. A. Longo, R. K. Petersen, J. B. Hansen, K. Kristiansen, and O. A. MacDougald. 2005. Effects of Wnt signaling on brown adipocyte differentiation and metabolism mediated by PGC-1{alpha}. *Mol. Cell. Biol.* **25:** 1272–1282.
31. Lomax, M. A., F. Sadiq, G. Karamanlidis, A. Karamitri, P. Trayhurn, and D. G. Hazlerigg. 2007. Ontogenic loss of brown adipose tissue sensitivity to {beta}-adrenergic stimulation in the ovine. *Endocrinology.* **148:** 461–468.
32. Yang, X., S. Enerback, and U. Smith. 2003. Reduced expression of FOXC2 and brown adipogenic genes in human subjects with insulin resistance. *Obes. Res.* **11:** 1182–1191.
33. Vantyghem, M. C., P. Pigny, C. A. Maurage, N. Rouaix-Emery, T. Stojkovic, J. M. Cuisset, A. Millaire, O. Lascols, P. Vermersch, J. L. Wemeau, et al. 2004. Patients with familial partial lipodystrophy of the Dunnigan type due to a LMNA R482W mutation show muscular and cardiac abnormalities. *J. Clin. Endocrinol. Metab.* **89:** 5337–5346.
34. Boguslavsky, R. L., C. L. Stewart, and H. J. Worman. 2006. Nuclear lamin A inhibits adipocyte differentiation: implications for Dunnigan-type familial partial lipodystrophy. *Hum. Mol. Genet.* **15:** 653–663.
35. Araujo-Vilar, D., L. Loidi, F. Dominguez, and J. Cabezas-Cerrato. 2003. Phenotypic gender differences in subjects with familial partial lipodystrophy (Dunnigan variety) due to a nuclear lamin A/C R482W mutation. *Horm. Metab. Res.* **35:** 29–35.
36. Haque, W. A., E. A. Oral, K. Dietz, A. M. Bowcock, A. K. Agarwal, and A. Garg. 2003. Risk factors for diabetes in familial partial lipodystrophy, Dunnigan variety. *Diabetes Care.* **26:** 1350–1355.
37. Ludtke, A., J. Genschel, G. Brabant, J. Bauditz, M. Taupitz, M. Koch, W. Wermke, H. J. Worman, and H. H. Schmidt. 2005. Hepatic steatosis in Dunnigan-type familial partial lipodystrophy. *Am. J. Gastroenterol.* **100:** 2218–2224.
38. Cannon, B., and J. Nedergaard. 2004. Brown adipose tissue: function and physiological significance. *Physiol. Rev.* **84:** 277–359.
39. Nedergaard, J., T. Bengtsson, and B. Cannon. 2007. Unexpected evidence for active brown adipose in adult humans. *Am. J. Physiol. Endocrinol. Metab.* **293:** E444–E452.
40. Johansen, K., M. H. Rasmussen, L. L. Kjems, and A. Astrup. 1995. An unusual type of familial lipodystrophy. *J. Clin. Endocrinol. Metab.* **80:** 3442–3446.
41. Ross, S. R., R. A. Graves, A. Greenstein, K. A. Platt, H. L. Shyu, B. Mellovitz, and B. M. Spiegelman. 1990. A fat-specific enhancer is the primary determinant of gene expression for adipocyte P2 in vivo. *Proc. Natl. Acad. Sci. USA.* **87:** 9590–9594.
42. Rosen, E. D., and B. M. Spiegelman. 2000. Molecular regulation of adipogenesis. *Annu. Rev. Cell Dev. Biol.* **16:** 145–171.
43. Lelliott, C. J., L. Logie, C. P. Sewter, D. Berger, P. Jani, F. Blows, S. O'Rahilly, and A. Vidal-Puig. 2002. Lamin expression in human adipose cells in relation to anatomical site and differentiation state. *J. Clin. Endocrinol. Metab.* **87:** 728–734.
44. Adams, M., C. T. Montague, J. B. Prins, J. C. Holder, S. A. Smith, L. Sanders, J. E. Digby, C. P. Sewter, M. A. Lazar, V. K. Chatterjee, et al. 1997. Activators of peroxisome proliferator-activated receptor gamma have depot-specific effects on human preadipocyte differentiation. *J. Clin. Invest.* **100:** 3149–3153.
45. Yanase, T., T. Yashiro, K. Takitani, S. Kato, S. Taniguchi, R. Takayanagi, and H. Nawata. 1997. Differential expression of PPAR gamma1 and gamma2 isoforms in human adipose tissue. *Biochem. Biophys. Res. Commun.* **233:** 320–324.
46. Tchkonia, T., N. Giorgadze, T. Pirtskhalava, Y. Tchoukalova, I. Karagiannides, R. A. Forse, M. DePonte, M. Stevenson, W. Guo, J. Han, et al. 2002. Fat depot origin affects adipogenesis in primary cultured and cloned human preadipocytes. *Am. J. Physiol. Regul. Integr. Comp. Physiol.* **282:** R1286–R1296.
47. Garg, A. 2000. Gender differences in the prevalence of metabolic complications in familial partial lipodystrophy (Dunnigan variety). *J. Clin. Endocrinol. Metab.* **85:** 1776–1782.
48. Haluzik, M., C. Colombo, O. Gavrilova, S. Chua, N. Wolf, M. Chen, B. Stannard, K. R. Dietz, D. Le Roith, and M. L. Reitman. 2004. Genetic background (C57BL/6J versus FVB/N) strongly influences the severity of diabetes and insulin resistance in ob/ob mice. *Endocrinology.* **145:** 3258–3264.
49. Ricci, M., M. Pellizzon, E. Ulman, J. Denier, and E. Arlund. 2005. Diet-induced obesity (DIO) is affected by level of dietary fat and gender in C57BL/6 mice. NAASO Annual Scientific Meeting, Vancouver, BC. 2005.
50. Burant, C. F., S. Sreenan, K. Hirano, T. A. Tai, J. Lohmiller, J. Lukens, N. O. Davidson, S. Ross, and R. A. Graves. 1997. Troglitazone action is independent of adipose tissue. *J. Clin. Invest.* **100:** 2900–2908.
51. Shimomura, I., R. E. Hammer, S. Ikemoto, M. S. Brown, and J. L. Goldstein. 1999. Leptin reverses insulin resistance and diabetes mellitus in mice with congenital lipodystrophy. *Nature.* **401:** 73–76.
52. Park, J. Y., O. Gavrilova, and P. Gorden. 2006. The clinical utility of leptin therapy in metabolic dysfunction. *Minerva Endocrinol.* **31:** 125–131.
53. Pajvani, U. B., M. E. Trujillo, T. P. Combs, P. Iyengar, L. Jelicks, K. A. Roth, R. N. Kitsis, and P. E. Scherer. 2005. Fat apoptosis through targeted activation of caspase 8: a new mouse model of inducible and reversible lipoatrophy. *Nat. Med.* **11:** 797–803.
54. Shum, B. O., C. R. Mackay, C. Z. Gorgun, M. J. Frost, R. K. Kumar, G. S. Hotamisligil, and M. S. Rolph. 2006. The adipocyte fatty acid-binding protein aP2 is required in allergic airway inflammation. *J. Clin. Invest.* **116:** 2183–2192.
55. Weisberg, S. P., D. McCann, M. Desai, M. Rosenbaum, R. L. Leibel, and A. W. Ferrante, Jr. 2003. Obesity is associated with macrophage accumulation in adipose tissue. *J. Clin. Invest.* **112:** 1796–1808.
56. Xu, H., G. T. Barnes, Q. Yang, G. Tan, D. Yang, C. J. Chou, J. Sole, A. Nichols, J. S. Ross, L. A. Tartaglia, et al. 2003. Chronic inflammation in fat plays a crucial role in the development of obesity-related insulin resistance. *J. Clin. Invest.* **112:** 1821–1830.